Available online at www.sciencedirect.com

ScienceDirect

Mendeleev Commun., 2023, **33**, 41–44

Mendeleev Communications

Electron density topology in Ca^{II}–Cu^{II} alanine hydroximate metallacrowns: crystal invariom *vs* DFT calculation

Roman V. Rumyantcev, Grigory Yu. Zhigulin, Galina S. Zabrodina, Marina A. Katkova, Sergey Yu. Ketkov and Georgy K. Fukin*

G. A. Razuvaev Institute of Organometallic Chemistry, Russian Academy of Sciences, 603137 Nizhny Novgorod, Russian Federation. E-mail: gera@iomc.ras.ru

DOI: 10.1016/j.mencom.2023.01.012

The first insight into the nature of intramolecular interactions in the Ca^{II}–Cu^{II} alanine hydroximate metallacrowns is provided on the basis of the invariom refinement and DFT calculations.

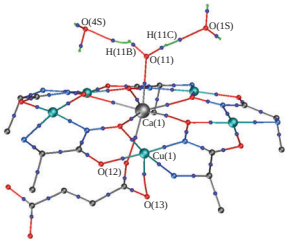

Keywords: metallacrown, alanine hydroximate, calcium(II), copper(II), X-ray diffraction, experimental–theoretical and theoretical electron density.

Among metallacrowns, the 15-metallacrown-5 (15-MC-5) family is the best example of inorganic crown ether analogs in terms of structure and functions. Rare-earth metal(III) 15-MC-5 complexes based on Cu^{II} ring metal ions with α-amino hydroximate ligands have been structurally characterized by single-crystal X-ray diffraction analysis.[1–8] In these complexes, the planar metallamacrocycle consists of five [Cu^{II}–N–O] repeat units with five hydroximate oxygen atoms surrounding a central lanthanide metal. The 15-MC-5 complexes with lighter lanthanides are more stable than those with heavier ones.[9] The relative stability of lanthanide amino hydroximate complexes has been determined by studying Ca^{II}–Ln^{III} substitution reactions.[10,11] The chemical behaviors of calcium and divalent lanthanide ions are similar because the effective ionic radius of Ca^{2+} (1.06 Å) is close to those of the trivalent light lanthanides Ce^{3+}, Pr^{3+} and Nd^{3+} (1.07, 1.05, and 1.04 Å, respectively).[12] Accordingly, by analogy to the light lanthanides, calcium can form similar 15-MC-5 compounds. Thus, the X-ray structures of Ca^{II}–Cu^{II} tryptophan hydroximate metallacrowns show that the central Ca^{2+} cation is well-encapsulated into the MC cavity with a maximum deviation from the oxygen mean plane of only 0.06 Å.[9] However, only few calcium metallacrowns have been characterized.[9,10,13] Here, we consider two Ca^{II}–Cu^{II} 15-MC-5 alanine hydroximate complexes containing polycarboxylate ligands in axial positions. They are of special interest due to the biological importance of Ca^{2+} binding to the carboxylate group. A study in this area can provide useful information on ion-binding structures of relevant biomolecules.[14] The biologically significant fumarate and isophthalate anions are convenient models for an analysis of Ca^{2+}–carboxylate bonding interactions. Not only geometries but also electronic structures should be examined for a deeper understanding of these interactions in the unique 15-MC-5 coordination environment. The alanine hydroximate ligands bear the simplest alkyl substituents providing chirality of the metallacrown.

The intra- and intermolecular interactions are characterized by an electron density distribution. However, it is extremely difficult to obtain ideal 15-MC-5 metallacrown crystals suitable for a precise X-ray diffraction study required for analyzing experimental electron density. On the other hand, Fukin and Cherkasov[15] demonstrated an excellent agreement between the topological characteristics of electron density in metal complexes obtained experimentally and theoretically (precise X-ray diffraction studies, crystal invariom, and DFT calculations). In this work, we used an asymmetric unit-cell aspherical scattering factor (a crystal invariom) and DFT calculations of isolated molecules to investigate electron density distribution in the Ca^{II}–Cu^{II} 15-MC-5 systems. A combination of the crystal invariom and DFT approaches is important in this case because of difficulties in reproducing geometrical characteristics (the metallacrown conformation, the concavity degree, and the flatness distortion) of these flexible molecules using only DFT calculations. The aim of this work was to synthesize Ca^{II}–Cu^{II} 15-MC-5 alanine hydroximate complexes with different anion ligands coordinated to the central Ca^{2+} ion and to study their molecular structures and the topological characteristics of electron density.

We used a modified two-step methodology based on a previously described synthetic procedure for water-soluble Sr^{II}–Cu^{II} 15-MC-5 metallacrowns.[16] At the first step, alanine hydroxamic acid and a calcium salt of isophthalic or fumaric acid were mixed in water, and $Cu(OAc)_2$ was added at the second step. The synthesized complexes $Ca(C_8H_4O_4)(H_2O)[15\text{-}MC_{Cu^{II}Alaha}\text{-}5](H_2O)_{16}$ **1** and $Ca(C_4H_2O_4)(H_2O)[15\text{-}MC_{Cu^{II}Alaha}\text{-}5](H_2O)_{15}$ **2** are air-stable and well soluble in water (for synthetic details, see Online Supplementary Materials). Both complexes crystallize in the $P2_12_12_1$ space group. Most likely, the system of crystal packing and H-bonding leads to the chiral orthorhombic space group. Chiral metallacrowns in the form of crystals belonging to such space groups have been prepared earlier with other amino hydroxamic acids (L-alanine-, L-phenylalanine-, and L-tyrosine hydroxamic acids).[2,10] The X-ray crystal structures of **1** and **2**

reveal the classic metallamacrocyclic 15-MC-5 configuration. [7] In both complexes, the central calcium ion is coordinated by five oxygen atoms of 15-MC-5, one oxygen atom of the isophthalate **1** or fumarate **2** anion, and one water molecule (Figure 1).† Thus, the Ca(1) coordination environment is a distorted pentagonal bipyramid. The hydroximate oxygen atoms of the metallacrown are located in the equatorial plane. The metallamacrocycle in complex **1** is almost flat, while its planarity is substantially distorted in complex **2**. The average deviations of hydroximate oxygen atoms from the plane are 0.042 and 0.126 Å in complexes **1** and **2**, respectively. Calcium atoms deviate from this plane by 0.137 and 0.230 Å in complexes **1** and **2**, respectively. The largest deviation of non-hydrogen atoms from the metallamacrocycle plane (except for the carbon atoms of Me groups) is 0.455 Å for **1** or 0.796 Å for **2**. The Ca–$O_{15\text{-MC-5}}$ distances vary in a range of 2.413(6)–2.546(3) Å. All main bond lengths in metallamacrocycle **1** are in a good agreement with those in complex **2** (Table S2) and previously published related compounds.[9,13,22]

The isophthalate anion in complex **1** is not planar. The dihedral angle between the planes of carboxyl groups is 17.71°.

† *Crystal data for* **1**. $C_{23}H_{68}CaCu_5N_{10}O_{31}$, M = 1338.65, orthorhombic, space group $P2_12_12_1$, 100(2) K, a = 15.5141(15), b = 16.7298(16) and c = 19.3080(19) Å, Z = 4, V = 5011.3(8) Å^3, d_{calc} = 1.774 g cm^{-3}, F_{000} = 2756. A black prism-shaped single crystal with dimensions of 0.27 × 0.10 × 0.08 mm was selected, and the intensities of 45084 reflections were measured using a Bruker D8 Quest diffractometer (ω-scans technique, λ[MoK_α] = 0.71073 Å, μ = 2.291 mm^{-1}, $2\theta_{max}$ = 58.260°). After merging of equivalents and absorption corrections, 13428 independent reflections (R_{int} = 0.0989) were used for the structure solution and refinement. Final R factors: R_1 = 0.0645 [8911 reflections with $I > 2\sigma(I)$], wR_2 = 0.1448 (all reflections), GOF = 1.032.

Crystal data for **2**. $C_{19}H_{64}CaCu_5N_{10}O_{30}$, M = 1270.58, orthorhombic, space group $P2_12_12_1$, 100(2) K, a = 15.5261(3), b = 16.5887(3) and c = 18.0577(4) Å, Z = 4, V = 4650.90(16) Å^3, d_{calc} = 1.815 g cm^{-3}, F_{000} = 2612. A black stick-shaped single crystal with dimensions of 0.46 × 0.10 × 0.09 mm was selected, and the intensities of 82344 reflections were measured using an Oxford Xcalibur Eos diffractometer (ω-scans technique, λ[MoK_α] = 0.71073 Å, μ = 2.461 mm^{-1}, $2\theta_{max}$ = 58.262°). After merging of equivalents and absorption corrections, 12493 independent reflections (R_{int} = 0.0784) were used for the structure solution and refinement. Final R factors: R_1 = 0.0353 [8911 reflections with $I > 2\sigma(I)$], wR_2 = 0.0840 (all reflections), GOF = 1.047.

The X-ray diffraction data for **1** and **2** were collected using the APEX3 (**1**) and CrysAlisPro (**2**) software packages. The intensity data were integrated by SAINT[17] (**1**) and CrysAlisPro[18] (**2**) programs. SADABS program[19] (**1**) and SCALE3 ABSPACK algorithm[17] (**2**) were used to perform absorption corrections. Both structures were solved by a dual method[20] and refined on F^2_{hkl} using the SHELXTL package.[21] All non-hydrogen atoms were refined anisotropically. The hydrogen atoms, except for the hydrogen atoms in water molecules, were placed in calculated positions and were refined in the riding model [U_{iso}(H) = 1.5 U_{eq}(C) for CH_3 groups and U_{iso}(H) = 1.2 U_{eq}(C) for other groups]. In turn, the hydrogen atoms in all water molecules in crystals **1** and **2** were found from Fourier syntheses of electron density. The asymmetric units of **1** and **2** contain 17 and 16 water molecules, respectively. Free refinement of hydrogen atoms in water molecules leads to unrealistic geometry and/or bad thermal ellipsoids. Further geometric (DFIX, SADI) and thermal [U_{iso}(H) = 1.2 U_{eq}(O)] constraints were imposed to maintain reasonable results. Thus, all O–H bond lengths in water molecules were fixed at the level of 0.96(1) Å. Therefore, when studying hydrogen bonds in structures **1** and **2**, we analyzed the geometry of the entire fragment D–H···A, where D is a hydrogen bond donor and A is an acceptor.

For the main crystallographic data and structure refinement details for complexes **1** and **2**, see Table S1 (Online Supplementary Materials).

CCDC 2168523 (**1**) and 2168524 (**2**) contain the supplementary crystallographic data for this paper. These data can be obtained free of charge from The Cambridge Crystallographic Data Centre *via* http://www.ccdc.cam.ac.uk.

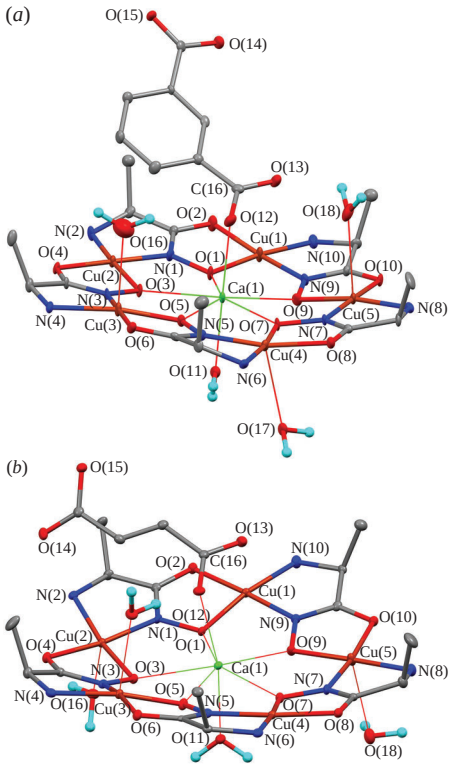

Figure 1 Molecular structures of complexes (*a*) **1** and (*b*) **2**. Thermal ellipsoids are at a 30% probability level. Hydrogen atoms are omitted for clarity.

In turn, the fumarate anion in complex **2** is even more significantly distorted. The dihedral angle between the planes of carboxyl groups in **2** is 41.13°. Uncoordinated carboxyl groups of isophthalate (**1**) and fumarate (**2**) anions take part in numerous intermolecular O···H interactions (Table S3). It is likely that the observed distortion of the carboxylate anions is a consequence of the hydrogen bonds formed. In both complexes, the distances between the C(16) atom of the carboxyl group and the oxygen O(12) atom directly bonded to the calcium atom are somewhat longer [1.269(11) and 1.270(6) Å] than the formal double bond C(16)=O(13) [1.241(11) and 1.257(6) Å]. In turn, the C(23)–O(14) and C(23)–O(15) distances of the second isophthalate carboxyl group in complex **1** are largely aligned with each other, and their values are intermediate [1.250(11) and 1.251(11) Å, respectively]. This behavior is typical for carboxylate anions.[23–25] Note that, in complex **2**, there is no significant equalization of C–O distances in the uncoordinated carboxyl group of the fumarate anion [1.246(6) and 1.285(6) Å]. Apparently, this is also associated with intermolecular O···H interactions in a crystal of **2**.

In crystals of **1** and **2**, the neighboring molecules of complexes are arranged in such a way that they form infinite molecular chains due to numerous intermolecular O···H interactions (Figure S1). As noted previously (see Figure S1), the metallamacrocycles in complexes **1** and **2** have different degrees of deviation from planarity. The different shapes of the metallamacrocycles in **1** and **2** can be caused by differences in the intermolecular interactions in the crystals. Despite the close cell parameters, complex **1** contains one more solvate water molecule compared to **2**. This leads to different intermolecular interactions in the crystals, which affect the shapes of the metallamacrocycles. The intermolecular N–H···O and O–H···O distances between neighboring metallacrowns in the crystals vary within ranges of 1.97(2)–2.22 and 1.97(2)–2.35(5) Å for complexes **1** and **2**, respectively. Neighboring chains of molecules are located almost perpendicular to each other in a crystal of **1**, and they are beveled

relative to each other at an angle of ~50° in a crystal of **2** (see Figure S2). Thus, the difference in the numbers of water molecules leads not only to different shapes of the metallacrowns but also to different locations of neighboring molecular chains in the crystals. Due to numerous water molecules in the crystals, a 3D network is formed in which the molecules are connected *via* hydrogen bonds (Table S3).

To study the electron density topology, we used an approach based on an asymmetric unit-cell aspherical scattering factor (a crystal invariom). Earlier, we found that this approach makes it possible to obtain adequate topological electron density characteristics in the coordination sphere of a metal atom[15] and to estimate the energies of intermolecular interactions.[26] The lone electron pairs of the five hydroximate oxygen atoms are directed towards the Ca(1) atom in **1** and **2** (Figure S3). The deformation electron densities (DED) of the O(12) lone electron pairs in the isophthalate and fumarate anions are directed towards the calcium atom in both **1** and **2** (Figure 2). A different situation is observed for the lone pairs of oxygen atoms of water molecules coordinated to the calcium atoms in **1** and **2**. The lone pairs of the O(11) atom in **1** deviate from the direction to the calcium atom, in contrast to those directed to Ca(1) in **2** (see Figure 2). This corresponds to the unsymmetrical coordination of the H_2O molecule to Ca(1) in complex **1** and more symmetric coordination of H_2O in **2** (see Figure 2). The Ca(1)O(11)H(11B)/Ca(1)O(11)H(11C) angles are 94.41°/160.41° in **1** and 128.83°/125.54° in **2** (Figure S3).

Another interesting feature of the DED distribution is observed in the CuONCO fragment of **1** and **2**. As can be seen in Figure 3, there is a DED depletion on the O(1)–N(1) bond instead of the expected concentration. Previously, a similar DED depletion was observed in a spiroendoperoxide antimony complex on the O–O bond.[27] In terms of the DED distribution, the Cu–O and Cu–N bonds correspond to the peak–hole interactions. We used the theory of Bader[28] to investigate the chemical bonds, water coordination, and charge distribution in **1** and **2**.

Molecular graphs of complexes **1** and **2** are shown in Figure S4. Water molecules coordinated to calcium atoms in **1** and **2** take part in the formation of hydrogen bonds with two neighboring H_2O molecules. However, the O···H distances and hydrogen bond energies in **1** (Table S4) are less uniform than those in **2**. According to the Espinosa–Molins–Lecomte correlation,[29] the differences in the energies of the O(1S)···H(11B) and O(8S)···H(11C) bonds are 5.3 and 2.4 kcal mol^{-1} in **1** and **2**, respectively. This leads to an unsymmetrical coordination of water molecules to the calcium atom in **1** as compared to **2**. Despite the difference in the coordination of water molecules, the Ca(1)–O(11) distances and the corresponding bond energies in **1** and **2** are very close (see Table S4).

An analysis of the electron density topology revealed the Cu(1)···O(13) interactions in **1** and **2** (Figure S5). Due to large

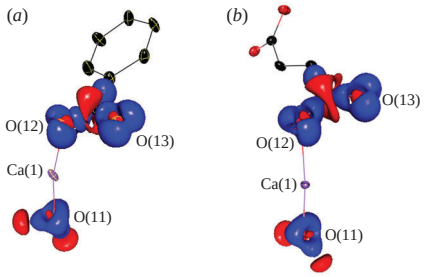

Figure 2 Isosurface (0.15 a.u.) of the deformation electron density (DED) on the water molecule and the C(16)O(12)O(13) fragment in (*a*) **1** and (*b*) **2**. The blue and red areas show the concentration of DED and the depletion of DED, respectively.

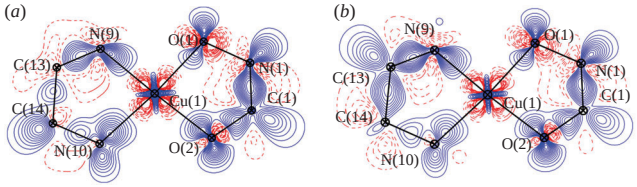

Figure 3 Experimental–theoretical DED sections (contour ±0.05 e Å^{-3}) in the Cu(1)O(1)O(2) plane of the fragments of (*a*) **1** and (*b*) **2**. The blue and red lines show the concentration of DED and the depletion of DED, respectively.

distances between copper and carbonyl oxygen in **1** [3.391(8) Å] and **2** [3.029(4)Å], these interactions cannot be detected in a geometric analysis. In addition, a weak Cu(2)···C(22) interaction [3.493(11) Å] is detected in complex **1**. Thus, the isophthalate anion in **1** and the fumarate anion in **2** can be formally considered as bidentate and tridentate ligands, respectively. Note that a geometric analysis of the Cu–O(H_2O) distances in **1** and **2** showed that only three water molecules are coordinated to the copper atoms (see Figure 1). According to the Cambridge Structural Data Bank,[30] the Cu–O(H_2O) distances vary in a wide range of 1.74(2)–2.921(13) Å.[31,32] The Cu(3)–O(16), Cu(4)–O(17), and Cu(5)–O(18) distances in **1** and Cu(2)–O(16), Cu(3)–O(17), and Cu(5)–O(18) distances in **2** vary from 2.375(4) to 2.715(4) Å (Table S5). Additional Cu–O(H_2O) contacts were localized when investigating the electron density topology in **1** and **2** (Figure S5). The Cu(1)–O(12S) [2.957(9) Å] and Cu(4)–O(11S) [3.156(9) Å] distances in **1** and the Cu(5)–O(7S) [2.982(5) Å] distance in **2** significantly exceed the geometric criteria for such interactions. Therefore, these interactions cannot be localized on the basis of the known Cu–O(H_2O) distances. The energies of interactions localized in the study of the electron density topology (0.7–1.8 kcal mol^{-1}) are significantly lower than those of the interactions predicted geometrically (3.2–9.2 kcal mol^{-1}).

According to Bader's theory,[28] the Ca–O(H_2O), Ca–O(15-MC-5), Ca–O(carboxylate), Cu–O(carboxylate), and Cu–O(H_2O) interactions in **1** and **2** are closed-shell interactions (Laplacian of electron density $\nabla^2\rho(\mathbf{r}_{cp}) > 0$; local electron energy density $h_e(\mathbf{r}_{cp}) > 0$, Tables S4, S5 and S6). Due to the fact that electron energy density values are nearly zero and the Winxpro program[33] does not calculate uncertainties of electron density topological characteristics, we consider that these interactions are boundary between intermediate [$(\nabla^2\rho(\mathbf{r}_{cp}) > 0$, $h_e(\mathbf{r}_{cp}) < 0$] interactions and closed-shell ones. The Cu–O and Cu–N contacts in the five-membered CuONCO and CuNCCN metallofragments (see Figure 3) correspond to intermediate interactions (Table S6). The DED depletion at the critical point (3, –1) on the O–N bond in the CuONCO fragment is caused by a positive value of the electron density Laplacian [$\nabla^2\rho(\mathbf{r}_{cp}) = 0.261$ a.u. in **1**]. Thus, the O–N interaction in the CuONCO fragment is intermediate [$(\nabla^2\rho(\mathbf{r}_{cp}) > 0$, $h_e(\mathbf{r}_{cp}) < 0$]. However, the electron density at the O–N bond CP (3, –1) [$\rho(\mathbf{r}_{cp}) = 0.312$ a.u. in **1**] is comparable to that for the O–C bond [$\rho(\mathbf{r}_{cp}) = 0.350$ a.u. in **1**], which is covalent [$\nabla^2\rho(\mathbf{r}_{cp}) < 0$, $h_e(\mathbf{r}_{cp}) < 0$]. A similar situation takes place in complex **2**. The invariom-based calcium charge (1.71 e in **1** and 1.78 e in **2**) reflects its state. The formally two-valent copper atoms bear lower positive charges (0.8–0.94 e in **1** and 0.84–0.87 e in **2**).

In order to understand how well the experimental–theoretical and theoretical electron density topologies agree to each other, we have performed DFT calculations of the molecules of **1** and **2**. To simplify the model, both solvate and coordinated water molecules on metal atoms were not included in the calculations. The optimized geometry of metallacrown **1** also revealed significant distortions of planarity (Figure S6). The largest

deviations of non-hydrogen atoms from the metallamacrocycle planes (except for the carbon atoms of Me groups) were 1.166 and 1.476 Å for the optimized molecules of **1** and **2**, respectively, which are much higher than that for molecules in the crystals (0.455 Å in **1** and 0.796 Å in **2**). Despite this fact, the coordination sphere of the central calcium atom was reproduced adequately. The calculated average deviations of oxygen atoms from the planes are 0.048 Å in **1** and 0.151 Å in **2**. Calcium atoms deviate from this plane by 0.343 and 0.328 Å in complexes **1** and **2**, respectively.

As follows from Table S6, differences in the topological characteristics of electron density for all interactions in **1** and **2** do not exceed the transferability index [$\rho(\mathbf{r}) = 0.015$ a.u. (0.1 e Å^{-3}), $\nabla^2\rho(\mathbf{r}) = 0.17$ a.u. (3–4 e Å^{-5})].[34] The exceptions are the values of $\nabla^2\rho(\mathbf{r})$ for O–N, O–C, N–C, and C–C bonds in the CuNCCN and CuONCO fragments of complexes **1** and **2**, and electron density [$\rho(\mathbf{r})$] at the N(10)–C(14) bond in **1**. We believe that the intermolecular interactions involving these atoms in the crystal lead to a substantial difference in the parameters $\nabla^2\rho(\mathbf{r})$ and $\rho(\mathbf{r})$ (Figure S7). Theoretical Bader's charges calculated for calcium (1.82 e in **1** and 1.81 e in **2**) and copper (1.17–1.21 e in **1** and 1.17–1.18 e in **2**) atoms are slightly more positive compared to the experimental–theoretical ones. As a result, the *d*-orbital populations obtained from DFT calculations are somewhat lower than the experimental–theoretical values (Table S7). Nevertheless, the experimental–theoretical and theoretical charges are in good agreement with each other.

In this study, we found that the distortion of the metallacrown planarity has no significant effect on the topological characteristics of experimental–theoretical or DFT-based electron density. Therefore, differences between the metallacrown shapes obtained from the X-ray experiments and DFT calculations are not crucial for an analysis of intramolecular interactions. The difference in the experimental–theoretical and theoretical topological characteristics of electron density [mainly $\nabla^2\rho(\mathbf{r})$] are caused by intermolecular interactions in the crystals.

This research was supported by the Russian Science Foundation (project no. 18-13-00356). The study was carried out using the equipment of the center for collective use 'Analytical Center of the IOMC RAS' with the financial support of the grant 'Ensuring the development of the material and technical infrastructure of the centers for collective use of scientific equipment' from the Ministry of Science and Higher Education of the Russian Federation (unique project identifier is RF2296.61321X0017, Agreement with the G. A. Razuvaev Institute of Organometallic Chemistry RAS no. 075-15-2021-670).

Online Supplementary Materials

Supplementary data associated with this article can be found in the online version at doi: 10.1016/j.mencom.2023.01.012.

References

1 M. S. Lah and V. L. Pecoraro, *Comments Inorg. Chem.*, 1990, **11**, 59.
2 J. J. Bodwin, A. D. Cutland, R. G. Malkani and V. L. Pecoraro, *Coord. Chem. Rev.*, 2001, **216**–**217**, 489.
3 G. Mezei, C. M. Zaleski and V. L. Pecoraro, *Chem. Rev.*, 2007, **107**, 4933.
4 M. Tegoni and M. Remelli, *Coord. Chem. Rev.*, 2012, **256**, 289.
5 M. Ostrowska, I. O. Fritsky, E. Gumienna-Kontecka and A. V. Pavlishchuk, *Coord. Chem. Rev.*, 2016, **327**–**328**, 304.
6 Y. Pavlyukh, E. Rentschler, H. J. Elmers, W. Hubner and G. Lefkidis, *Phys. Rev*., 2018, **B97**, 214408.
7 M. A. Katkova, *Russ. J. Coord. Chem.*, 2018, **44**, 284 (*Koord. Khim.*, 2018, **44**, 135).
8 G. Mezei, C. M. Zaleski and V. L. Pecoraro, *Chem. Rev.*, 2007, **107**, 4933.
9 M. Tegoni, M. Furlotti, M. Tropiano, C. S. Lim and V. L. Pecoraro, *Inorg. Chem.*, 2010, **49**, 5190.
10 C. S. Lim, M. Tegoni, T. Jakusch, J. W. Kampf and V. L. Pecoraro, *Inorg. Chem.*, 2012, **51**, 11533.
11 G. Yu. Zhigulin, G. S. Zabrodina, M. A. Katkova and S. Yu. Ketkov, *Russ. Chem. Bull.*, 2019, **68**, 743.
12 B. Martin and F. S. Richardson, *Q. Rev. Biophys.*, 1979, **12**, 181.
13 I. S. Safyanova, I. A. Golenya, V. A. Pavlenko, E. Gumienna-Kontecka, V. I. Pekhnyo, V. V. Bon and I. O. Fritsky, *Z. Anorg. Allg. Chem.*, 2015, **641**, 2326.
14 E. A. Grzybowska, *Biomolecules*, 2018, **8**, 42.
15 G. K. Fukin and A. V. Cherkasov, *Mendeleev Commun.*, 2021, **31**, 182.
16 M. A. Katkova, G. S. Zabrodina, G. Yu. Zhigulin, E. V. Baranov, M. M. Trigub, A. A. Terentiev and S. Yu. Ketkov, *Dalton Trans.*, 2019, **48**, 10479.
17 *SAINT, Data Reduction and Correction Program*, Bruker, Madison, WI, 2014.
18 *CrysAlisPro Software System, Version 1.171.38.46*, Rigaku Oxford Diffraction, Rigaku Corporation, Wroclaw, Poland, 2015.
19 L. Krause, R. Herbst-Irmer, G. M. Sheldrick and D. Stalke, *J. Appl. Crystallogr.*, 2015, **48**, 3.
20 G. M. Sheldrick, *Acta Crystallogr., Sect. A: Found. Adv.*, 2015, **71**, 3.
21 G. M. Sheldrick, *Acta Crystallogr., Sect. C: Struct. Chem.*, 2015, **71**, 3.
22 M. A. Katkova, G. S. Zabrodina, E. V. Baranov, M. S. Muravyeva, E. A. Kluev, A. S. Shavyrin, G. Yu. Zhigulin and S. Yu. Ketkov, *Appl. Organomet. Chem*., 2018, **32**, e4389.
23 R. V. Rumyantcev, N. V. Zolotareva, O. V. Novikova, B. I. Petrov, N. M. Lazarev and V. V. Semenov, *Crystallogr. Rep.*, 2021, **66**, 441.
24 A. V. Pavlishchuk, S. V. Kolotilov, M. Zeller, L. K. Thompson and A. W. Addison, *Inorg. Chem.*, 2014, **53**, 1320.
25 A. V. Pavlishchuk, S. V. Kolotilov, M. Zeller, S. E. Lofland, L. E. Thompson, A. W. Addison and V. Hunter, *Inorg. Chem*., 2017, **56**, 13152.
26 T. S. Pochekutova, G. K. Fukin, E. V. Baranov, B. I. Petrov, N. M. Lazarev and V. K. Khamylov, *Inorg. Chim. Acta*, 2022, **531**, 120734.
27 G. K. Fukin, M. A. Samsonov, E. V. Baranov, A. I. Poddel'skii and V. K. Cherkasov, *Russ. J. Coord. Chem.*, 2017, **43**, 858 (*Koord. Khim.*, 2017, **43**, 759).
28 R. F. W. Bader, *Atoms in Molecules: A Quantum Theory*, Oxford University Press, 1990.
29 E. Espinosa, E. Molins and C. Lecomte, *Chem. Phys. Lett.*, 1998, **285**, 170.
30 I. J. Bruno, J. C. Cole, P. R. Edgington, M. Kessler, C. F. Macrae, P. McCabe, J. Pearson and R. Taylor, *Acta Crystallogr.*, 2002, **B58**, 389.
31 X. Wang, H. Hu, A. Tian, H. Lin, J. Li and L. Shi, *Inorg. Chem. Commun.*, 2010, **13**, 745.
32 L. A. Dubraja, I. Jerić, A. Puškarić, J. Bronić and E. Moreno-Pineda, *CrystEngComm*, 2018, **20**, 2396.
33 A. Stash and V. Tsirelson, *J. Appl. Crystallogr.*, 2002, **35**, 371.
34 L. Checinska, S. Mebs, C. B. Hubschle, D. Forster, W. Morgenroth and P. Luger, *Org. Biomol. Chem*., 2006, **4**, 3242.

Received: 1st June 2022; Com. 22/6920